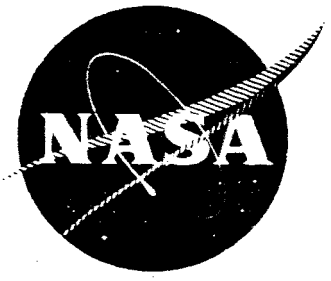

NASA CR-54193

SECOND QUARTERLY REPORT
PRESSURE MEASURING SYSTEMS FOR CLOSED CYCLE LIQUID METAL FACILITIES

Edited by
Richard E. Engdahl

PREPARED FOR
NATIONAL AERONAUTICS AND SPACE ADMINISTRATION
CONTRACT NAS 3-4170
September 28, 1964

CONSOLIDATED CONTROLS CORP.
BETHEL, CONNECTICUT

NOTICE

This report was prepared as an account of Government sponsored work. Neither the United States, nor the National Aeronautics and Space Administraion (NASA), nor any person acting on behalf of NASA:

A.) Makes any warranty or representation, expressed or implied, with respect to the accuracy, completeness, or usefulness of the information contained in this report, or that the use of any information, apparatus, method, or process disclosed in this report may not infringe privately owned rights; or

B.) Assumes any liabilities with respect to the use of, or for damages resulting from the use of any information, apparatus, method or process disclosed in this report.

As used above, "person acting on behalf of NASA" includes any employee or contractor of NASA, or employee of such contractor, to the extent that such employee or contractor of NASA, or employer of such contractor prepares, disseminates, or provides access to, any information pursuant to his employment or contract with NASA, or his employment with such contractor.

Requests for copies of this report should be referred to:

National Aeronautics and Space Administration
Office of Scientific and Technical Information
Washington, D. C. 20546
Attention: AFSS-A

NASA CR-54193
CCC-443

SECOND QUARTERLY REPORT
June 1--August 31, 1964

PRESSURE MEASURING SYSTEMS FOR CLOSED CYCLE LIQUID METAL FACILITIES

Edited by
Richard E. Engdahl

PREPARED FOR

NATIONAL AERONAUTICS AND SPACE ADMINISTRATION

CONTRACT NAS 3-4170

SEPTEMBER 28, 1964

Technical Management
NASA - Lewis Research Center
Nuclear Power Technology Branch
R. N. Weltmann

Consolidated Controls Corporation
Bethel, Connecticut

FOREWORD

The major contributors to this development program are Mr. R. Engdahl, Project Manager, Mr. Anthony Cassano, Mr. David Mends, Mr. Charles Schoenfeld and Mr. William Waller.

ABSTRACT

33376

Continuing development of a series of pressure transducers for liquid metal systems is described. Problems encountered in fabricating the pressure capsule are outlined along with the anticipated solutions. The experimental program for completing the evaluation of the thermionic and variable impedance detector systems is described. Some details of the test facility are discussed. These include the liquid potassium test capsules and the method of measuring diaphragm deflection.

Author

TABLE OF CONTENTS

TABLE OF CONTENTS (Cont'd)

LIST OF ILLUSTRATIONS

LIST OF TABLES

1.0 Introduction

The objective of Contract NAS 3-4170 is to develop a series of pressure transducer equipment compatible with advanced closed cycle power systems. These systems utilize liquid metals such as mercury, sodium, potassium and other alkali metals as working and heat transfer media at elevated temperatures. Pressure measurements in the high temperature liquid, vapor, and two phase streams will be required for research, design and control purposes for SNAP-8 and other liquid metal space power systems. Since small pressure changes might indicate the onset of instability, instruments are required that can follow and record minute changes. In addition, space flight requires light-weight pressure measuring systems capable of enduring long periods of unattended operation.

Eight pressure ranges are included in this work covering both absolute and differential pressure instruments. The absolute ranges are 0-5,

0-20, 0-80, 0-300, and 0-500 psia. The differential pressure ranges include ±1, ±5, and ±20 psid at static pressures to 300 psia. All systems are to include overload protection to 100 percent of range.

Liquid metal pressure measurements at elevated temperatures pose many problems which challenge the designer and demand the best from available materials. To establish a firm design base for the complete series of transducers, four materials and two transducer systems will be evaluated.

These design data will then be incorporated into a series of transducers covering the eight instrument ranges defined above. The selected material and signal transduction system will be developed for use as either ground or flight hardware.

2.0 Summary

Progress in the design and fabrication of the FS-85, C129Y, W-25Re and T-222 pressure capsules is presented. Using the simplified capsule design with spark discharge machined discs, FS-85 and C129Y alloy capsules have been assembled and sectioned to determine the weld soundness and depth of weld penetration. Work on the W-25Re alloy capsule has involved similar weld sample tests and the development of a transition piece between the capsule and the columbium pressurization system. Work on the T-222 alloy capsule is awaiting delivery of this material.

The experimental thermionic transducer has been designed, built, and is now undergoing initial check out. The only apparent problem has been a heater failure during the initial vacuum chamber bake-out. Steps are being taken to correct the deficiency.

The analysis of the variable impedance sensor resulted in expressions requiring computer

solutions. An alternative experimental program has been developed which will obtain the data needed to proceed with the evaluation of the variable impedance device. In addition, the experiments will provide data on the skin depth phenomena which, at present, must be assumed in the analytic treatment. A pancake coil-diaphragm mock-up has been fabricated and initial experiments have been conducted. Resonance effects introduced by instrument impedances made these tests inconclusive. Further tests, using a Q-meter instrument, have corrected this situation.

Five electrical terminals have been built and tested at 1800°F and up to 300 psia internal pressure. The results are presented along with a review of additional testing performed in the very high vacuum test facility (10^{-8} Torr).

The multiple station test facility is basically complete. The system has been cleaned and baked out in preparation for the insertion of

the test capsules. The only remaining work is the mounting of the camera and the final piping of the argon pressurization system.

3.0 Design and Fabrication of Pressure Element

Work is progressing on the FS-85, C129Y and W-25Re alloy capsules. The T-222 alloy material is not yet delivered. The necessary electron-beam welding techniques are being developed along with efforts to supplement available welding facilities.

Diaphragm capsules were assembled from FS-85 and C129Y alloys, photographs of which are shown in Figure 1, but when these capsules were sectioned to determine the depth of weld penetration it was found that insufficient penetration had been obtained. A section of the FS-85 capsule is shown in Figure 2.

Work on these capsules has been delayed by scheduling problems in the electron-beam welding facilities. Alternate sources are being investigated in order to speed up the program.

A number of attempts have been made to electron-beam weld FS-85 columbium alloy tubing (pressurization system) to the W-25Re alloy (pressure capsule),

but in every case the weld showed cracking. It is felt that the cracking in the weld was probably caused by diffusion of Cb, Ta, etc. into the W-25Re alloy, decreasing the solid solubility of Re in W so that some σ phase was formed. The W-Re equilibrium diagram (Reference 1) is shown in Figure 3, where it is seen that the W-25Re alloy lies very close to the $\beta / \beta + \sigma$ phase boundary which is at 26 percent Re at 1500°C.

The next approach was to employ a weld insert of a dissimilar metal between the W-25Re and the FS-85 alloy in an attempt to overcome the weld cracking. Inserts of Cb-1Zr, molybdenum, rhenium, Mo-50Re were fabricated and mock-ups were made by electron beam welding as shown in Figure 4. Metallographic sections of the welds are shown in Figure 5. It is seen that in every case the welds were cracked, the only exception being the W-25Re to the Mo-50Re insert.

A possible explanation for the success of the W-25Re to Mo-50Re welds may be found in the

ternary equilibrium diagram for W-Mo-Re (Reference 2) shown in Figure 6. It will be seen that any conceivable alloy combination of W, Mo and Re which might result from melting together W-25Re and Mo-50Re must fall within the alpha single phase area (corresponding to the β phase area in the W-Re binary diagram, Figure 3) bounded by the points Mo-W-Y-Z in Figure 6, and will lie to the left of the $\alpha/\alpha + \sigma$ phase boundary, YZ. Therefore, no σ phase should occur in the weld.

The Mo-50Re insert was cracked where it was welded to the FS-85. This suggested the possibility of using a Mo-50Re tube for making the connection between the pressurization system and the capsule. Another insert of Mo-50Re was successfully welded to W-25Re. Accordingly, several pieces of Mo-50Re tubing were obtained, and an attempt is being made to assemble a W-25Re capsule in this manner.

Another technique considered was to make the tube from W-3Re alloy which might prove weldable

to W-25Re. This material is available in rod form. The intention was to make the rod into a tube by spark discharge machining.

A sample of W-3Re rod (0.250 inch diameter) was ordered, and was found to be broken into several fragments as a result of damage during shipping. Subsequent discussion with the vendor revealed that the ductile/brittle transformation temperature of this alloy is about 150°C in a rod of this diameter, and that this transformation is below room temperature only in heavily worked wire. This material was obviously unsuitable for use in the pressure transducer.

The simplified form of diaphragm capsule is presently being assembled as shown in Figure 7B. In this design the diaphragms are machined from thicker material, and it will be seen that the simplified design comprises a tube and four discs with only four welds. The original design shown in Figure 7A comprised a tube plus eleven parts

and required eleven welds. It is proposed to assemble any future W-25Re capsules according to the simplified design, the discs being spark discharge machined.

4.0 Deflection - Electrical Signal

The analysis of the thermionic and variable impedance detector systems has been completed and is fully presented in the First Quarterly Report (Reference 3). Emphasis has now shifted to an experimental approach to confirm the anticipated performance of the thermionic diode and to obtain data needed to proceed with the evaluation of the variable impedance device.

4.1 Thermionic Diode Sensor

A dual emitter thermionic test device has been designed. Figure 8 presents an assembly view of the dual diode and Figure 9 shows the device installed in one of the test facility vacuum chambers. The emitters are Philips Type B tungsten dispenser cathodes (0.120 inch diameter, 0.040 inch thick) with standard barium oxide and aluminum oxide impregnation. The reference collector is mechanically fixed 0.006 inch from its emitter. The active collector-emitter distance is adjustable between 0.004 and 0.006 inch by means of the micrometer assembly mounted on the top vacuum flange. Electrical connections for the diode heater power as well as the emitters and collectors are made using feed-through terminals installed in this flange. Nickel rods (0.1 inch diameter) extend from the feed-through terminals down into the test chamber to the diode where connections are made to the various device elements.

A tungsten wire (0.012 inch diameter) formed to fit the cavity between the two emitters serves as the heater. The cavity and the heater are individually plasma sprayed with aluminum oxide to electrically insulate the heater from the emitters. Tests have established the ability of the heater to raise the emitter assembly to the desired operating temperature of 2100°F (1420°K).

4.1.1 Test Circuitry and Instrumentation

The thermionic diode system described in the First Quarterly Report may be simulated by the test circuitry shown in Figure 10.

The object of the experiment is to determine the linearity achieved between active collector distance and the difference current ($i_a - i_r$) when the sum-of-the-currents ($i_a + i_r$) is held constant by adjusting the voltage V. Calculations have indicated that this linearity is about 3 percent when ($i_a + i_r$) is maintained at a value of 144 milliamperes. This corresponds to an active collector distance of 0.006 inch, a voltage V of 20 volts and an emitter temperature of 1420°K. The possibility of improving the linearity by having ($i_a + i_r$) vary with active collector position will also be investigated. Although the difference current amplifier and the feedback regulated power supply mentioned in the First Quarterly Report will not be used in this system, all the current and voltage values will be measured and correlated

with the analysis. These data should then provide the information needed to formulate the signal conditioning equipment requirements.

An equally important phase of the program will involve the determination of errors introduced by changes in operating parameters. The parameters of interest are emitter temperature (monitored by pyrometry through the test chamber viewing window and adjusted by changing the heater input level) and the voltage V applied to the collectors (monitored by a voltmeter and potentiometer adjusted). Analysis has indicated that errors introduced by reasonable changes in these parameters will be minimal. Experimental verification would be valuable and of considerable importance in selecting the preferred detector system.

4.1.2 Preliminary Test Results

The first test assembly failed following the initial bakeout in the vacuum chamber. This bakeout is at 1800°F where the temperature is raised to this value in stages with the restriction that the pressure in the test chamber shall not exceed 10^{-6} Torr. This precaution is necessary to avoid emitter poisoning and the resultant loss of emission capability. Preliminary checks indicated an open circuit heater. Post mortem examination revealed that the spot weld joints between the tungsten heater leads and the nickel feed-through rods had opened. In addition, the tungsten wire broke inside the emitter assembly and made effective repair of the device impossible. It is felt that excessive embrittlement of the tungsten wire due to the bakeout was at fault.

The second test assembly, presently in progress, will incorporate modifications to solve the problems mentioned above. The tungsten heater will be replaced by a heater which is more ductile and less

liable to embrittlement upon heating. In addition, the heater leads will have ceramic tubing to protect them inside the emitter sandwich. This tubing will terminate outside the sandwich assembly. Also, a flexible transition connection will be used between the heater wire and the nickel rod to absorb any mechanical strain generated during the cool-down period.

4.2 Impedance Bridge Sensor

In order to evaluate the analytical approach presented in Appendix C of the First Quarterly Report, an attempt has been made to determine, by slide rule calculations, the inductance of a single turn pancake coil in the presence of a conducting diaphragm. The details of this effort are found in Appendix B. The conclusion obtained was that the analytical approach would not yield results unless a computer is utilized.

Two alternatives present themselves. One would be to use the computer and the other to use an experimental program to complete the analysis. The experimental program is preferred since it would complete the design data needed and also shows promise of providing the skin depth values which must be assumed in the computer program.

4.2.1 Experimental Program

The main objective of the experimental program will be the determination of pancake coil inductance as a function of diaphragm position. In addition, it is expected that the program will result in data that will verify the basic premise of the analysis; the presence of an image coil whose position is determined by a skin-depth phenomena. The discussion that follows expands upon this last statement.

Image theory has been proposed as a valid method of determining the coil inductance. Of prime importance is the distance between the pancake coil and the image coil. This distance is in turn determined by a skin depth phenomena experienced in the diaphragm. At some effective skin depth (which may be postulated to be some multiple of a unit skin depth) inside the diaphragm, the induction field of the pancake coil will tend to zero and the pancake and image coils become equidistant from this plane. This phenomena is

dependent upon the resistivity of the diaphragm material. As an example, consider a perfectly conducting diaphragm (resistivity = 0). The field does not enter the diaphragm at all and has its zero value at the diaphragm surface. For this case the pancake coil to image coil distance will be twice the pancake coil to diaphragm distance. In addition, the pancake coil inductance will vary between a value of zero when the distance is zero and a finite value, e.g. L_{∞}, corresponding to complete absence of a diaphragm. The inductance L will tend to this value as the spacing increases. Although the exact shape of the curve is uncertain, Figure 11 indicates the general trend. The fact that $L = 0$ at $d_c = 0$ for $\rho_{r1} = 0$ means that the pancake and image coils are so close to each other that their axial fields cancel out in the plane of the pancake coil.

Now, an important point must be made. The pancake coil inductance is determined by the opposing interaction of two axial induction fields; one due

to the pancake coil itself and the other due to the image coil. The strength of the image field is governed by the distance between the coils. This distance is determined by two parameters; the diaphragm spacing and the effective skin depth as established by the diaphragm resistivity. However, the sum of diaphragm spacing and effective skin depth is the important thing. In other words, two diaphragms of different resistivities will result in the same pancake coil inductance if the diaphragm spacing is adjusted to compensate for the difference in effective skin depth. As resistivity increases, skin depth increases. Referring to Figure 11, the inductance L_2 for a spacing d_{c2} with a zero resistivity diaphragm would correspond to the same inductance L_2 caused by a diaphragm with zero spacing and an effective skin depth of $1/2\ d_{c2}$ determined by a finite resistivity ρ_{r2}. This statement applies also to inductance L_3 where a diaphragm with zero spacing would have an effective skin depth of $1/2 d_{c3}$ determined by resistivity

ρ_{r3}. If a diaphragm of very low resistivity (e.g. copper) is used, the $\rho_{r1} = 0$ curve will be approached. Using this curve, an effort may be made to determine correlations between effective skin depth and resistivity. Using the standard formula for unit skin depth as a function of resistivity, an effort will be made to determine whether the effective skin depth postulated above is a constant multiple of the unit skin depth.

The use of diaphragms of various resistivities should result in a series of parallel curves intersecting the ordinate at larger values of inductance for larger values of resistivities. This procedure will give an estimate of inductance change with diaphragm temperature. A temperature change will result in a resistivity change affecting skin depth and inductance even at constant spacing.

4.2.2 Preliminary Test Results

A 20 turn single-layer pancake coil (I.D. = 3/16 inch, O.D. = 9/16 inch, AWG 32 heavy Formvar insulated magnet wire) has been fabricated and encapsulated in the surface of a block of lucite. Diaphragm mock-ups of various materials covering a range of resistivity values and thicknesses (copper, 1.7 X 10^{-6} ohm-cm, 0.015 inch; cupro-nickel, 39 X 10^{-6} ohm-cm, 0.031 inch; monel, 49 X 10^{-6} ohm-cm, 0.015 inch; K-monel, 58 X 10^{-6} ohm-cm, 0.021 inch) have been prepared and mounted on polystyrene rods. A test fixture has been constructed to allow mounting of the diaphragm samples in a support slide and positioning of the samples at various distances from the coil by means of a vernier micrometer. Figure 12 shows the test fixture.

Initial testing of the coil on the basis of impedance measurements proved inconsistent. This testing involved the use of a radio frequency signal generator and a calibrated oscilloscope

to obtain current and voltage parameters. Parallel resonance phenomena introduced by the impedance characteristics of the instruments made this method inconclusive.

The test coil must be considered as a parallel LC circuit element. This requires that two unknowns, L and C, be evaluated. While it may be assumed that the capacitance C is relatively constant, the inductance L is certainly a function of diaphragm spacing and, according to the proposed analytical model, a function of circuit frequency. For this reason, an independent determination of C will be used to fix one of the unknowns and the other unknown, L, can then be obtained from either resonance or impedance data.

Preliminary tests, using a Q-meter instrument, have eliminated the resonance problem mentioned above. Capacitance and inductance values for the coil parameters will be obtained from this system.

5.0 Electrical Terminal

Five terminals have been built and tested at 1800°F and up to 300 psia internal pressure. This testing was performed to establish the joint strength and thus supply design data for the final test terminal. The strongest unit lasted 4 hours at the maximum condition. It was noted that there was an oxide problem that apparently lowered the joint strength. Therefore, it was decided to terminate the series of tests until brazing and testing could be conducted in the 10^{-8} Torr test environment. (See Section 6.0.) Table 1 presents the test results.

TABLE 1
ELECTRICAL TERMINAL TEST RESULTS

Unit No.	Max. Press.(psia)	Time @ Temp.	Location of Failure
14	300	4 hrs.-1800°F	Break in ceramic joint
15	150	5 min.-1400°F	Tubulation failed
16	300	20 min.-1800°F	Break in ceramic joint
17	300	17 min.-1800°F	Break in ceramic joint
18	---	----------	Not leak tight when first brazed

It should be noted that the test pressure was applied from the inside of the terminal, and therefore, the stress in the joint was much more than if the pressure had been applied externally.

Additional terminal tests were performed in August in the Vacuum Test Facility. Oxide formation appeared to be eliminated but no improvement in joint strength was observed. Means for raising the remelt temperature of the braze are being investigated as a solution to this problem. Also a terminal design which would reduce the joint stress is being evaluated.

A group of terminals have been ordered for inclusion in this test program. Figure 13 illustrates this design.

6.0 Vacuum Test Facility

The basic design concepts of the multiple station test facility are contained in the First Quarterly Report. During this report period, substantial progress has been made in the construction of the facility, which is now basically complete. The system has been cleaned and baked out in preparation for the insertion of the test capsules. The only remaining work is the mounting of the camera and the final piping of the argon pressurization system. A photograph of the facility is given in Figure 14. Preliminary tests have resulted in manifold vacuum measurements of 2×10^{-9} Torr at room temperature and 2×10^{-8} Torr with one vacuum chamber heated to 1800°F.

6.1.1 Facility Design - Liquid Metal Capsule

A procedure has been formulated for filling the compatibility test capsules with potassium. Consolidated Controls Corporation will fabricate the capsules and supply them to a qualified outside organization which will perform the following tasks:

1. Charge the capsules with potassium under vacuum, and seal the capsules by electron-beam welding. Supply an analysis of the potassium used. Return the capsules to CCC for testing.
2. After testing at CCC, open the capsules, completely remove the potassium contained and analyze the potassium for impurities. Return the capsules along with the impurity reports to CCC.

6.1.2 Facility Design - Diaphragm Deflection Measurement

A major problem has been to find a technique for measuring the motion of the diaphragm to an accuracy of 1 percent of the total travel. A total travel of 0.002 inch requires the motion to be measured to an accuracy of 20 microinches.

Initial tests to determine the distance between two scribed lines revealed that the above accuracy (±20 microinches) could not be obtained by direct observation. Parallax errors, caused by movement of the observer's eye, together with the difficulty of positively identifying one particular pair of lines, dictated the use of a photographic technique to produce a photograph from which measurements could be taken.

In the photographic system, there are two sources of error, the optical system and the film itself. The optical system may be analyzed by considering the fineness of detail, or resolution, of the objective lens. This analysis, as it

applies to the present experimental set-up using a binocular microscope with a 4 inch working distance, is contained in Appendix C. A reasonable estimate of the maximum attainable resolution of this system is 360 microinches. However, this is an optical system error dependent upon parameters such as objective illumination, working distance, lens diameter, etc. Assuming that these parameters are held fairly constant, the error will also be constant over a number of photographs.

Of more immediate concern is the error introduced by the film itself (film dimensional stability, intrinsic resolution capability of the film, and emulsion response to both the light input and the development procedures). These effects will appear as reproducibility errors between photographs taken of identical objects under identical conditions.

The binocular microscope is equipped with a direct illuminator which reduces the working distance from 4 inches to 3 inches. Since the

test piece will be approximately 3.5 inches from the viewing window, the working distance of the camera system must be greater than this distance. The illuminator was therefore modified so that the working distance was increased to 3.75 inches.

A number of photographs were taken of a pair of scribed lines at nominal 30X and 40X magnification using the binocular microscope and a camera filled with Polaroid film. The distances between the images of the lines on the photographs thus produced were measured at 7X magnification by means of the binocular microscope fitted with a filar eyepiece. Differences of several hundred microinches were observed between successive identical photographs.

To overcome this difficulty, glass metallographic plates were used. Preliminary tests using the glass plates indicate that the individual plate can be read to an accuracy of 7-15 microinches. However, as in the case of the Polaroid film, differences were observed in measurements taken

between the same lines on different photographs. This reproducibility error, while not as severe as with the Polaroid film, was about 200 microinches. Present work is aimed at refinement of this latter technique and evaluation of the reproducibility error.

Several preliminary tests have been made using a mechanical system to amplify the diaphragm movement by a factor of about 10. Using this system, the reproducibility error of 200 microinches will be reduced to 20 microinches, assuming no other uncertainties. Figure 15 shows the system installed in a vacuum test chamber. Both the preliminary test mock-up and a pressure capsule installation are shown.

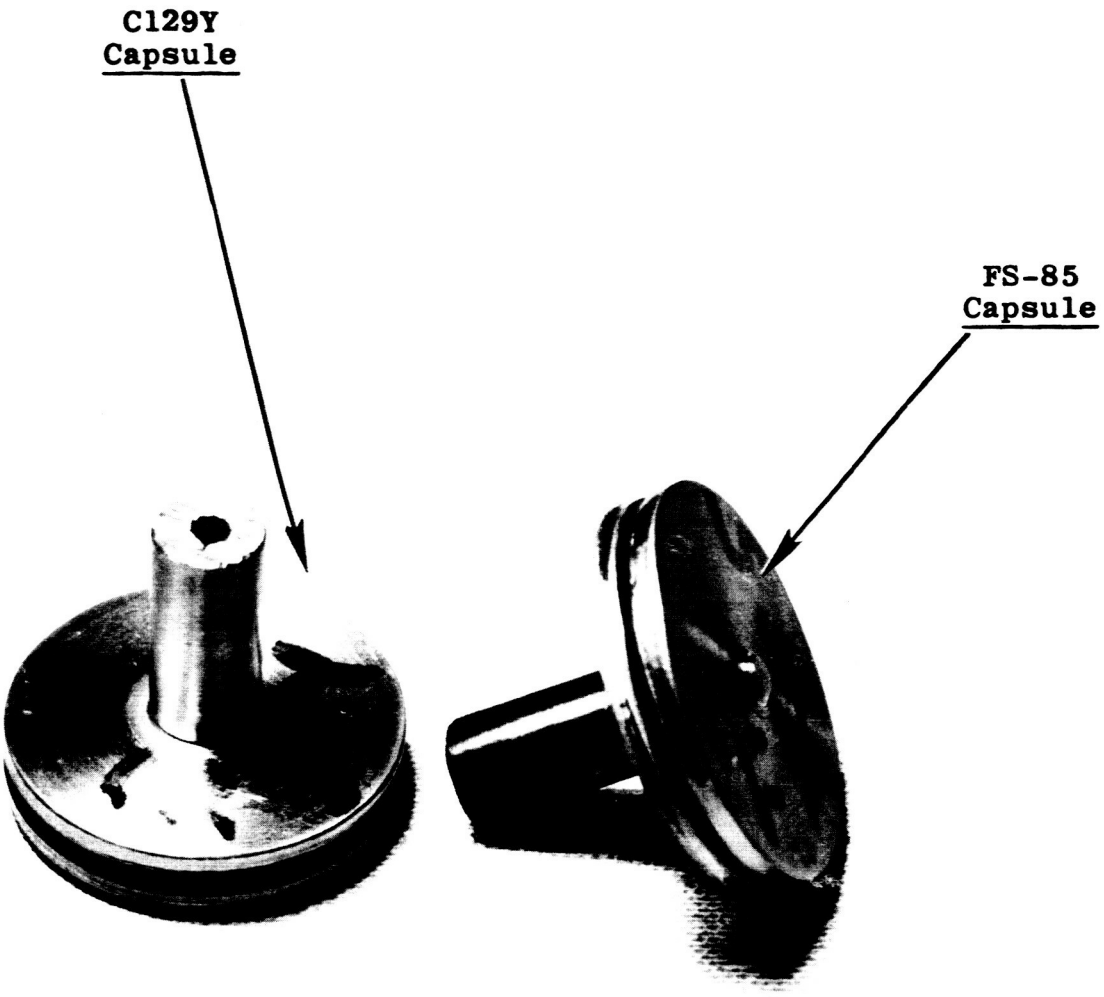

Figure 1

FS-85, C129Y Diaphragm Capsules

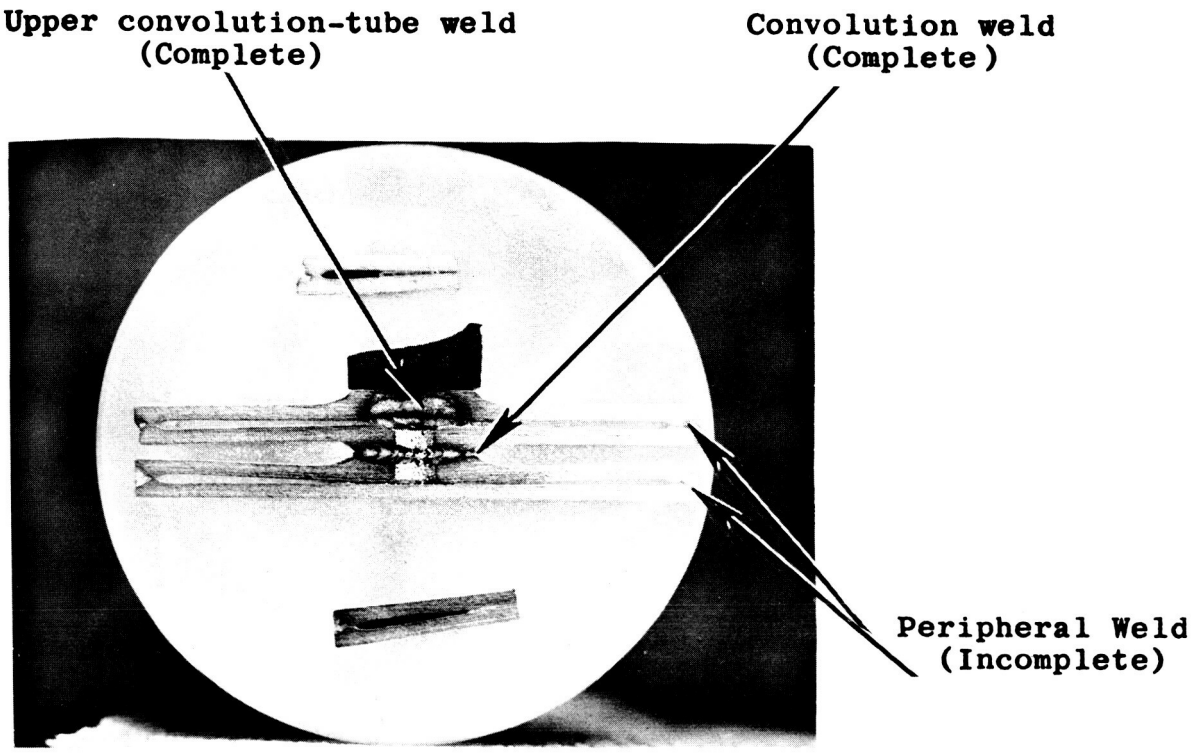

Section cut parallel to capsule diameter.
Slight distortion occurred during mounting.

Figure 2

Weld Section of FS-85 Capsule

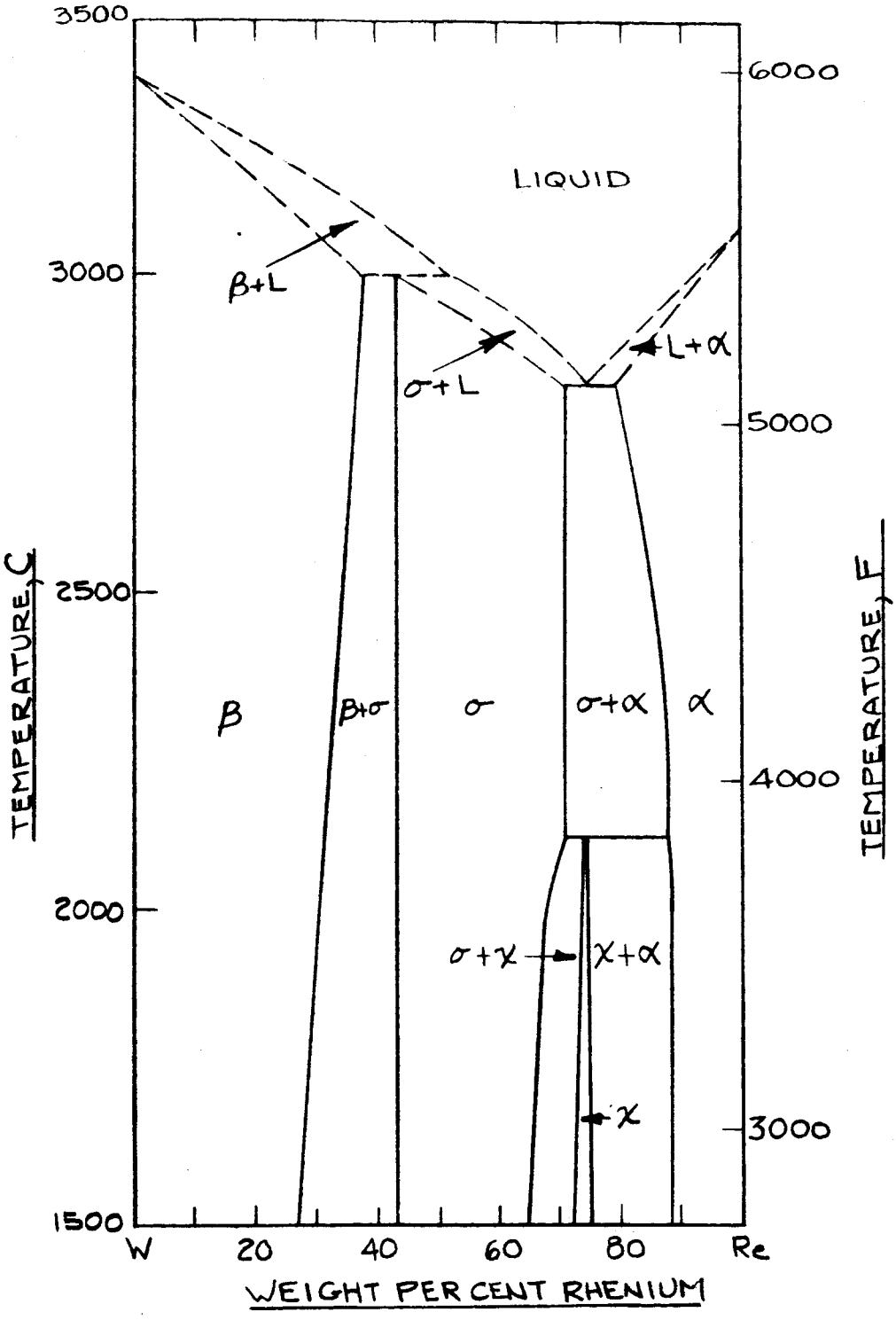

Figure 3

W-Re Binary Equilibrium Diagram

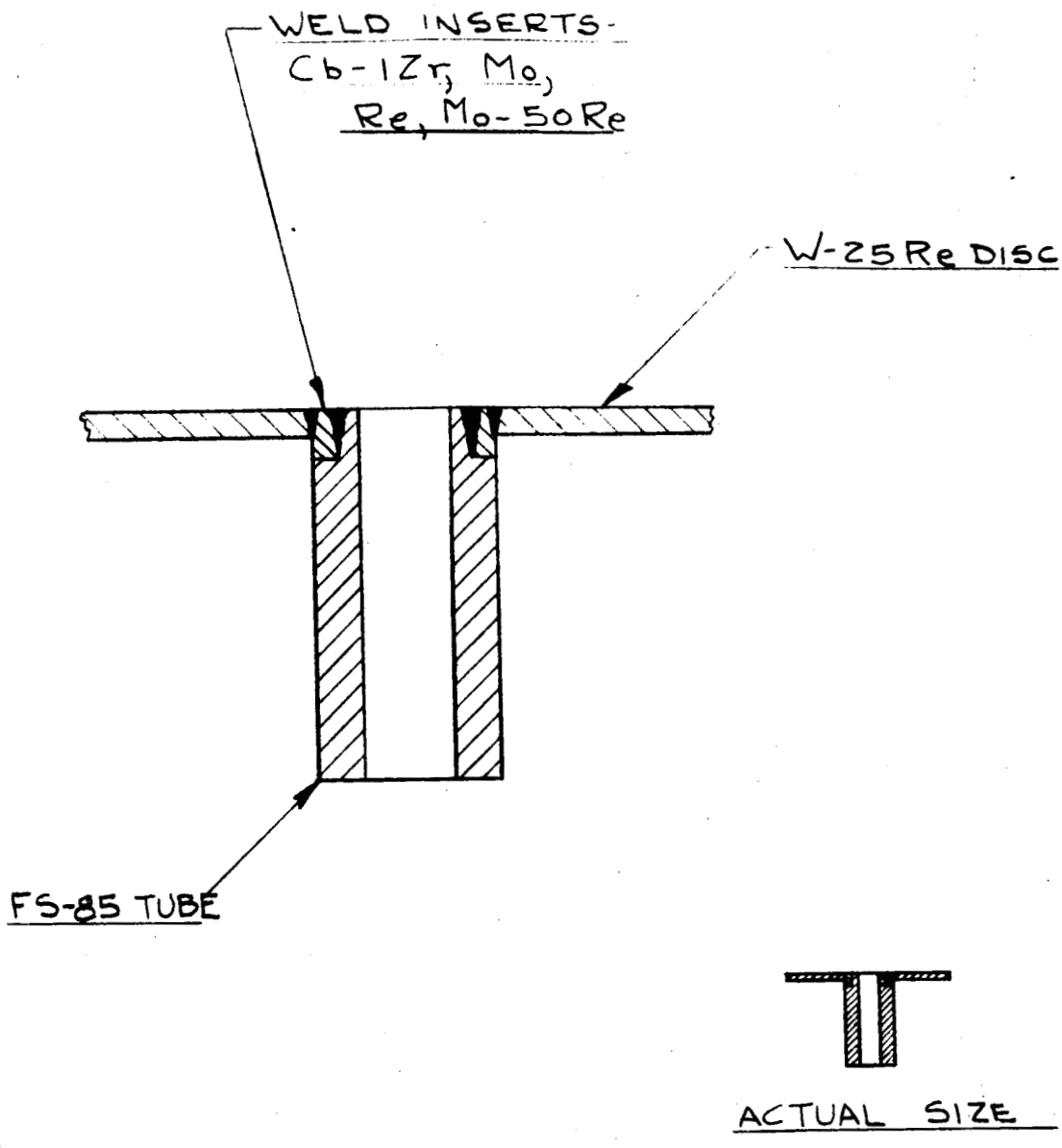

Figure 4

E-B Weld Mock-ups Using Various Inserts

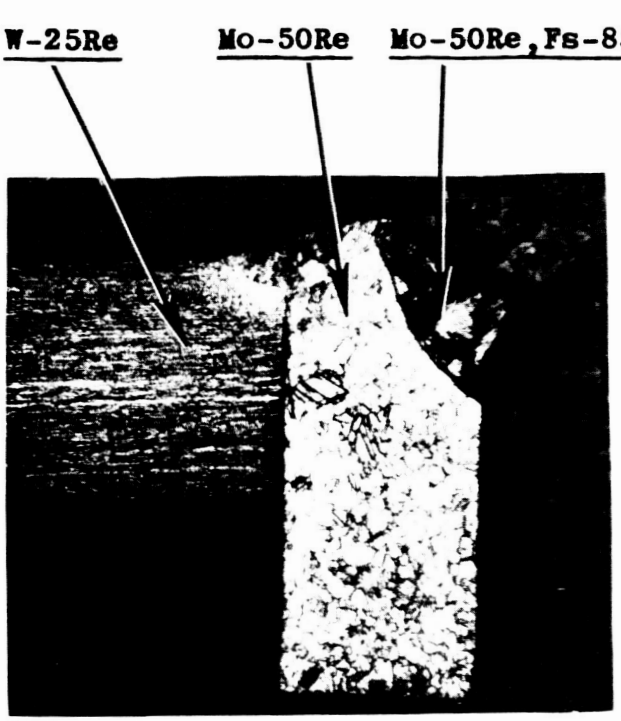

W-25Re,Mo-50Re weld incomplete. Mo-50Re,FS-85 weld broke off but intermetallic compounds and shattered weld are evident.

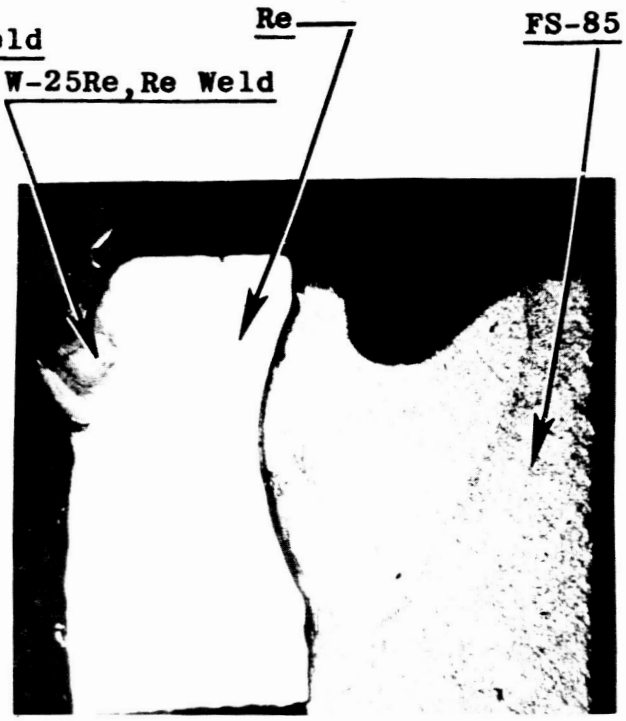

W-25Re,Re weld cracked and broke during sectioning. Re,FS-85 weld complete.

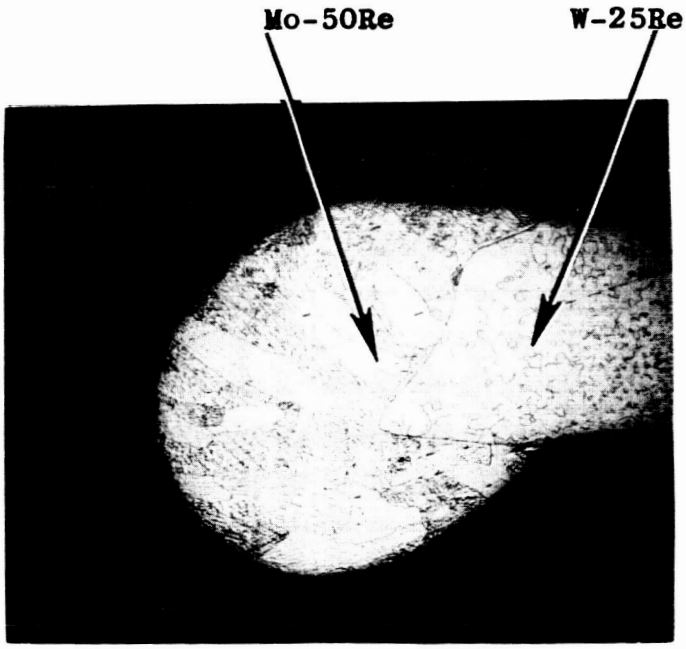

Complete Weld

Figure 5

Metallographic Sections of Welds

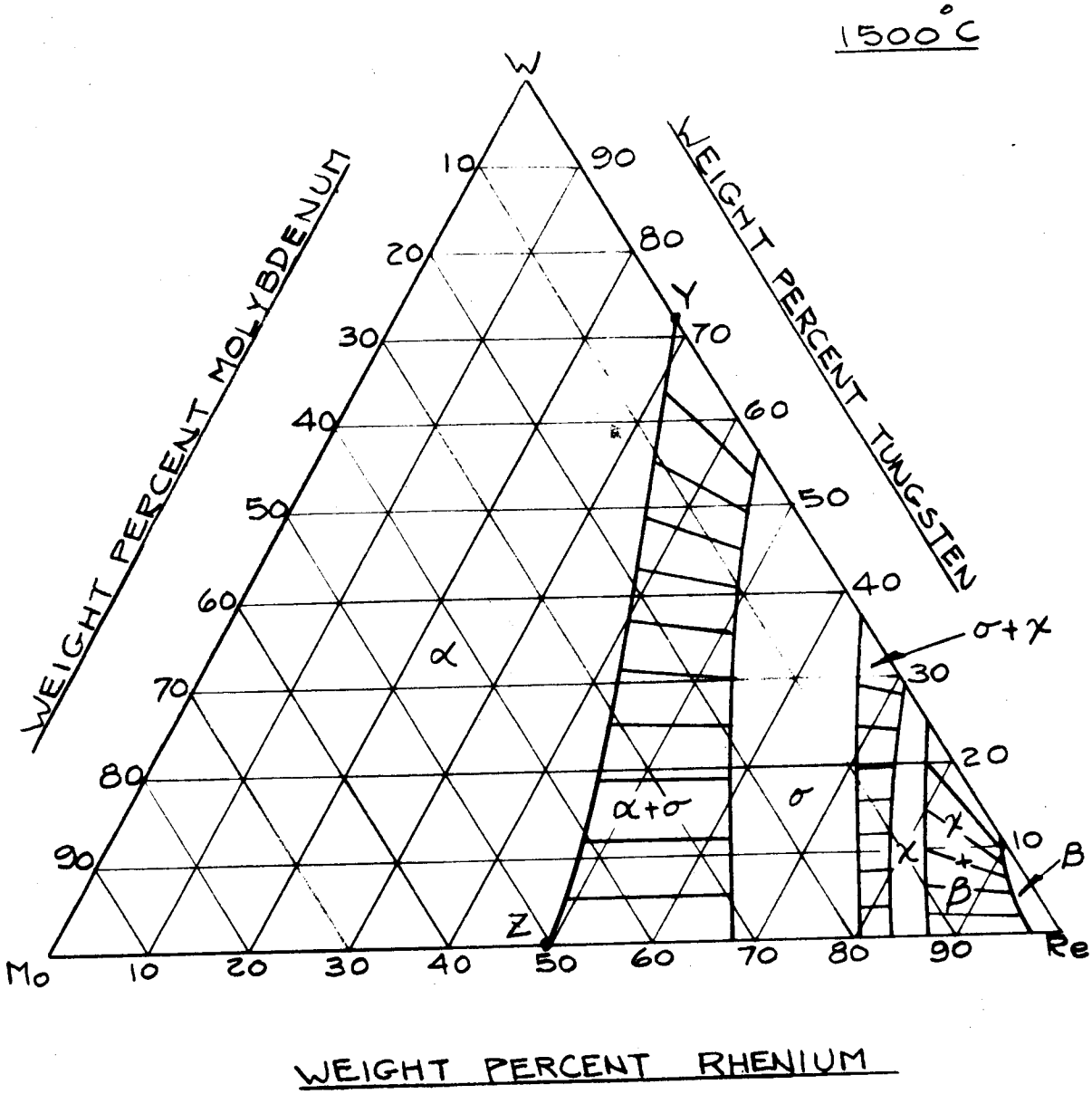

Figure 6

W-Mo-Re Ternary Equilibrium Diagram

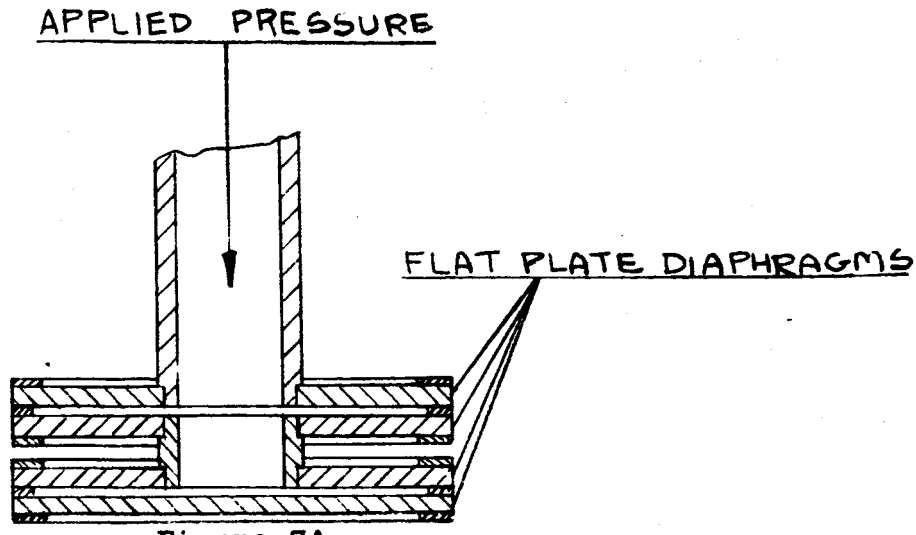

Figure 7A
Ring Plate Diaphragm Design

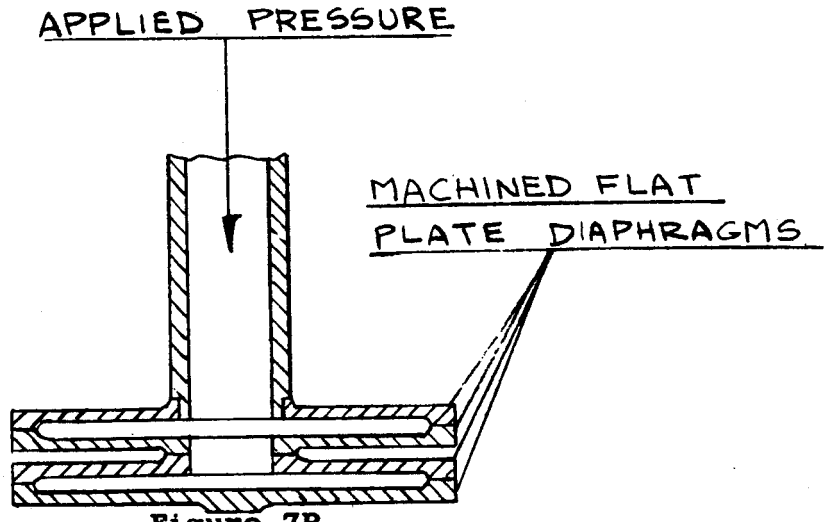

Figure 7B
Machined Diaphragm Design

Figure 7

Diaphragm Capsule Design

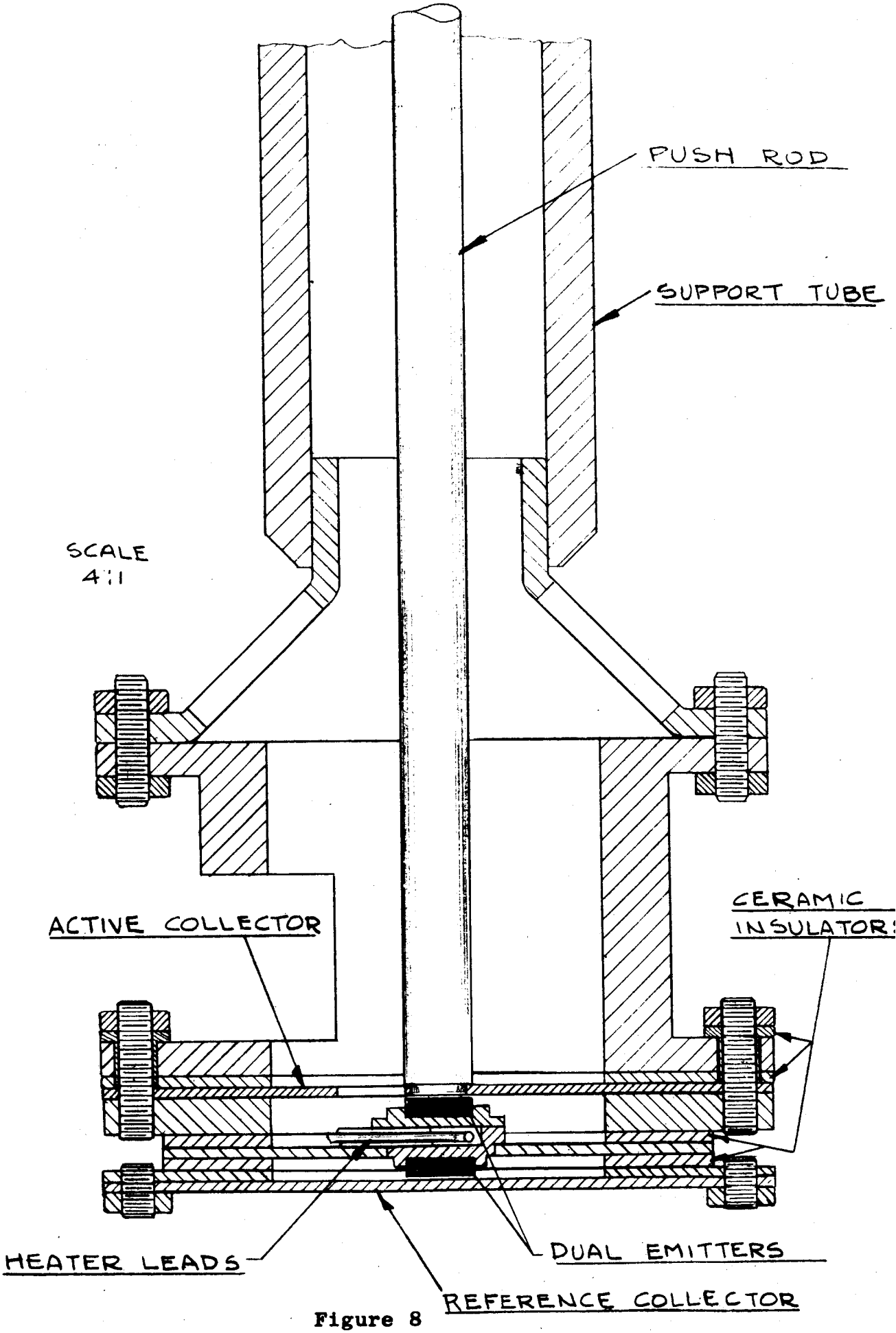

Figure 8

Dual Emitter Test Device

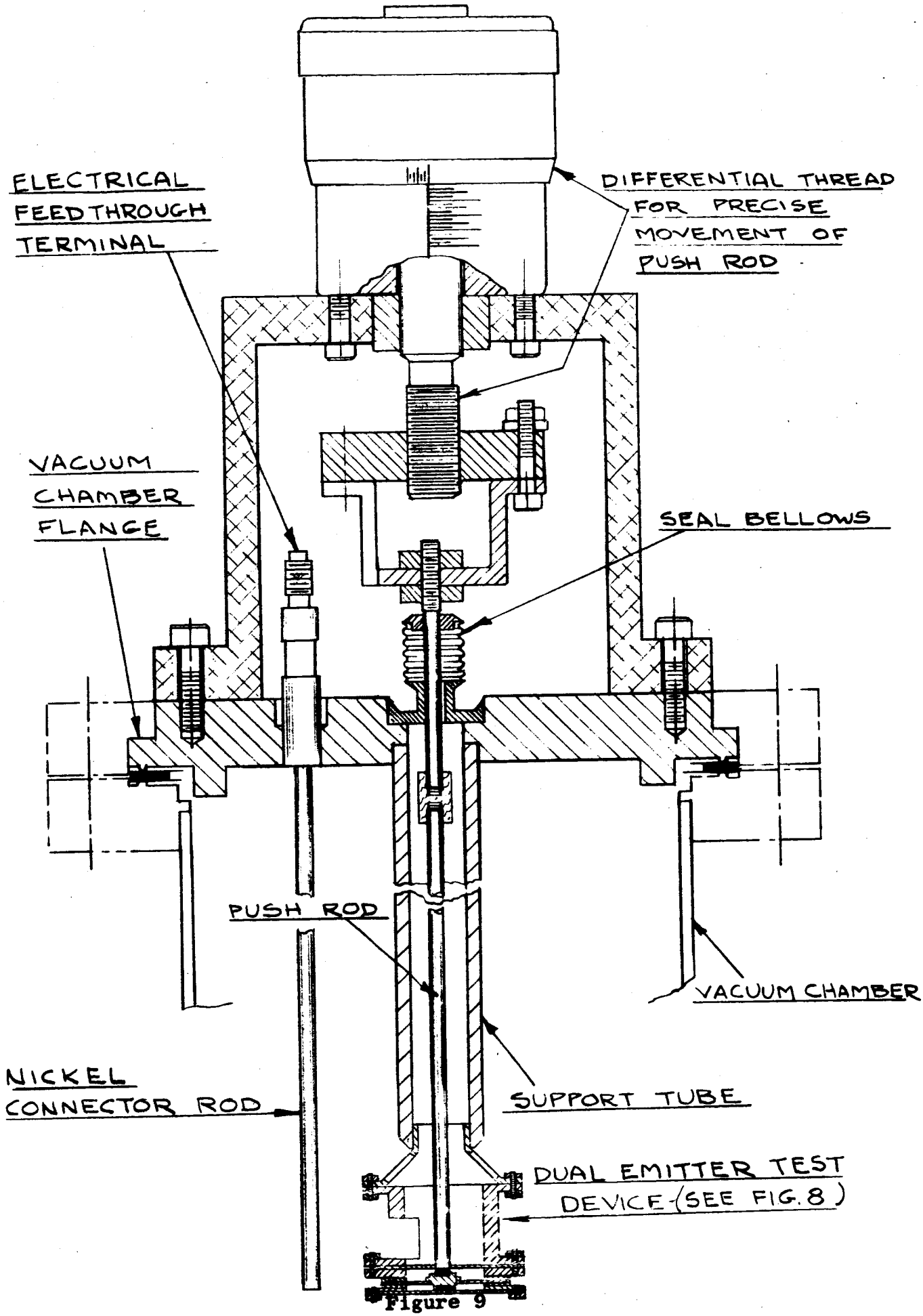

Figure 9

Dual Emitter Test Device - Vacuum Chamber Installation

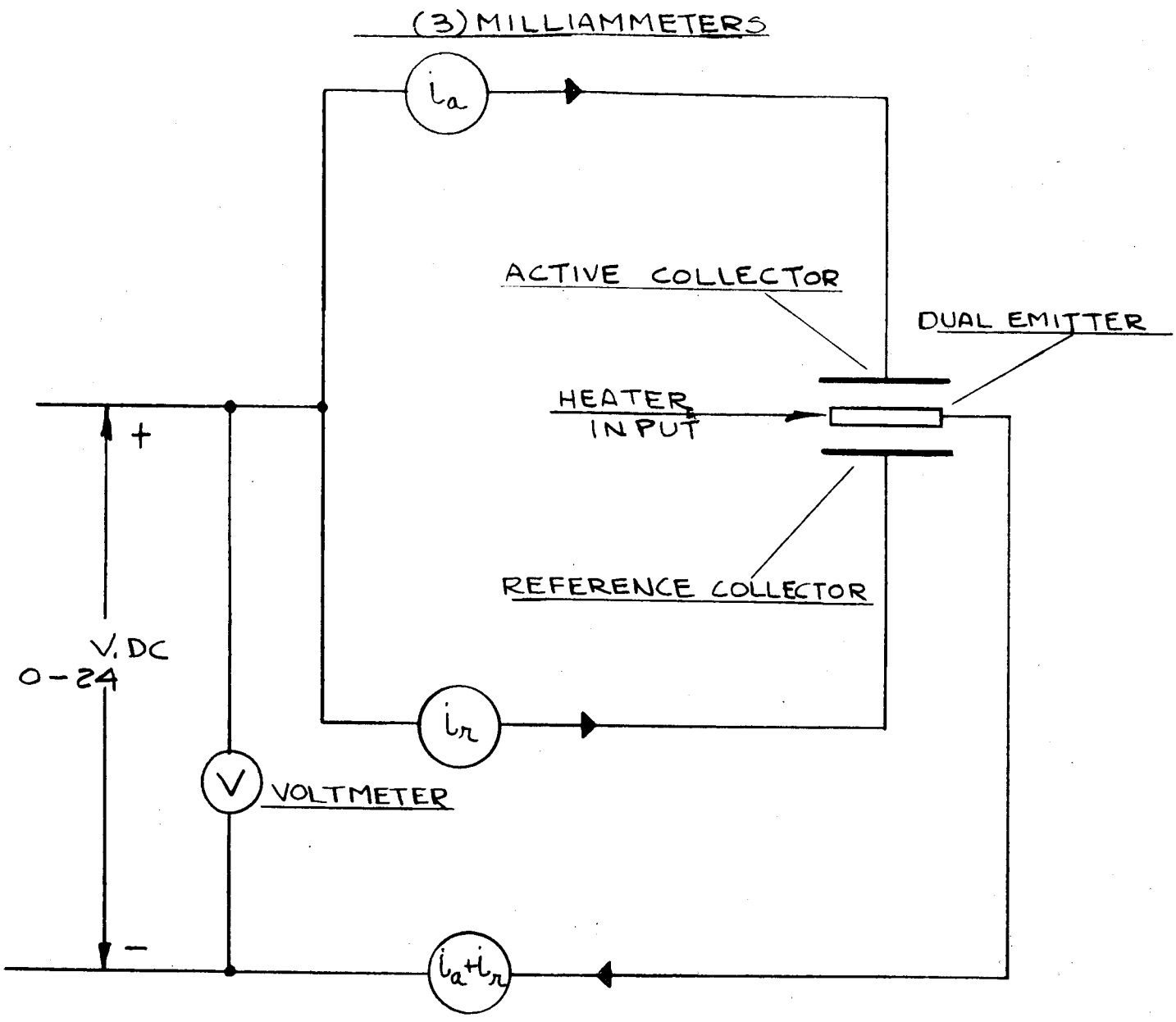

Figure 10

Thermionic Test Circuitry

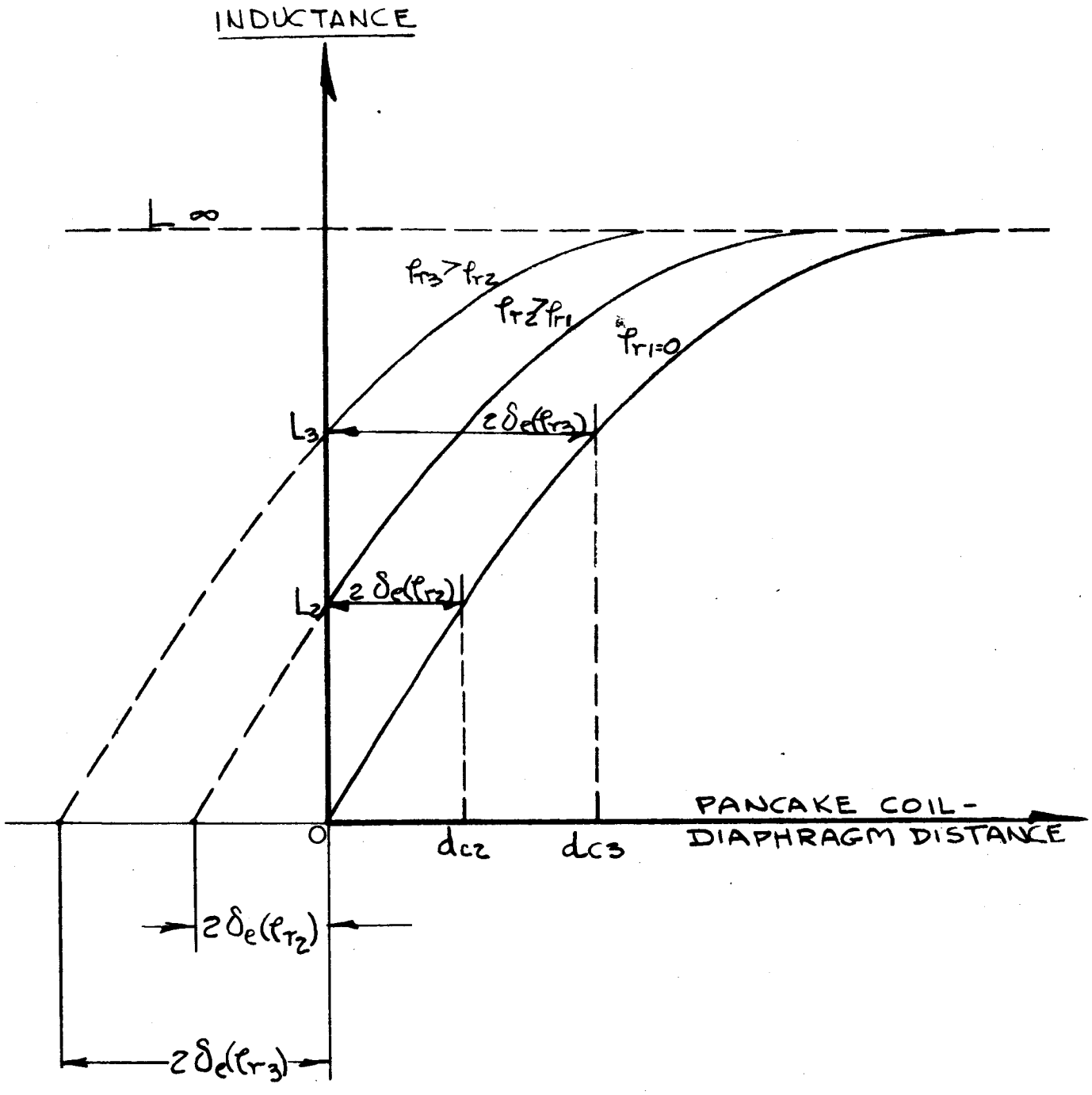

Figure 11

Inductance-Distance Characteristics

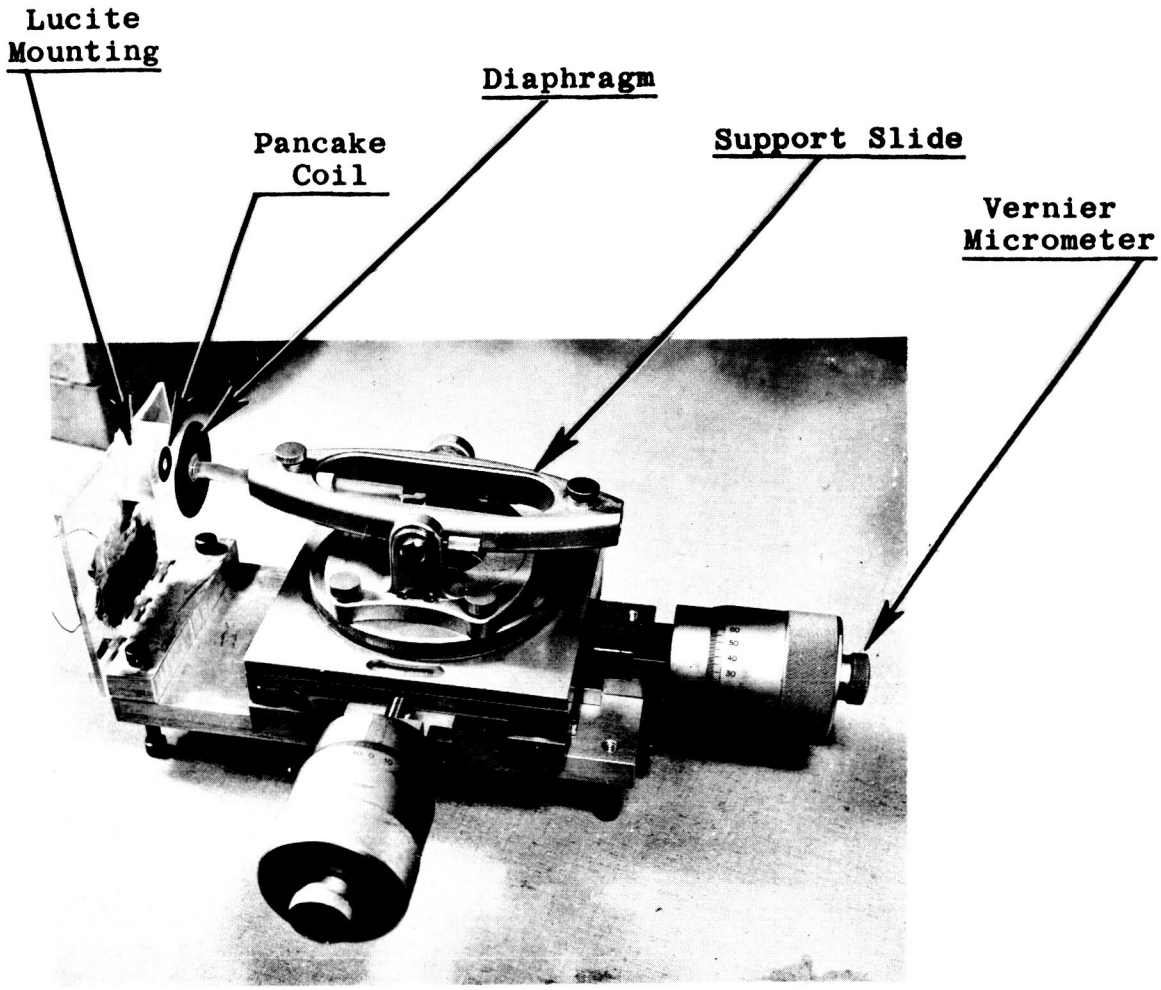

Figure 12

Variable Impedance Test Fixture

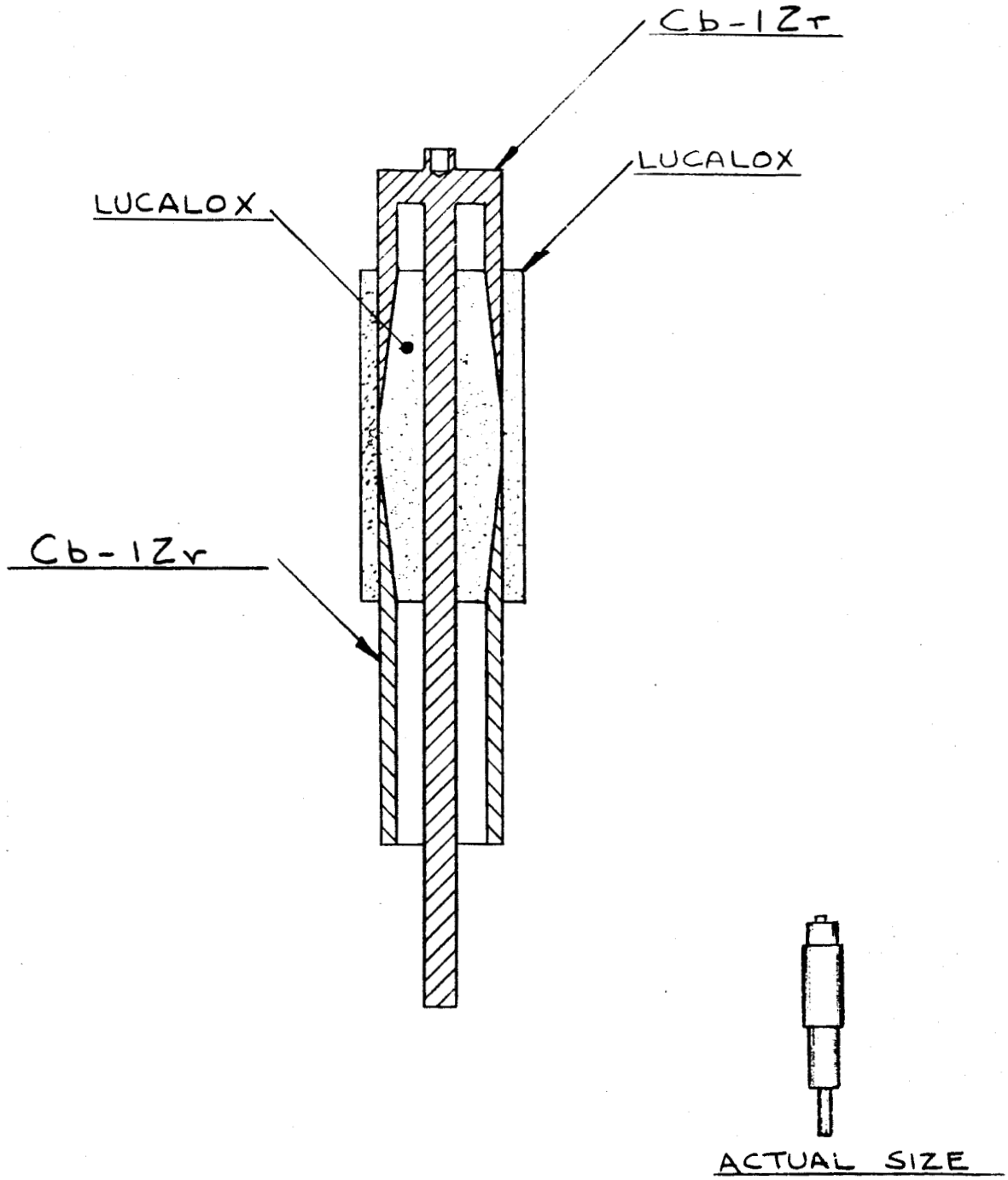

Figure 13

Electrical Terminal

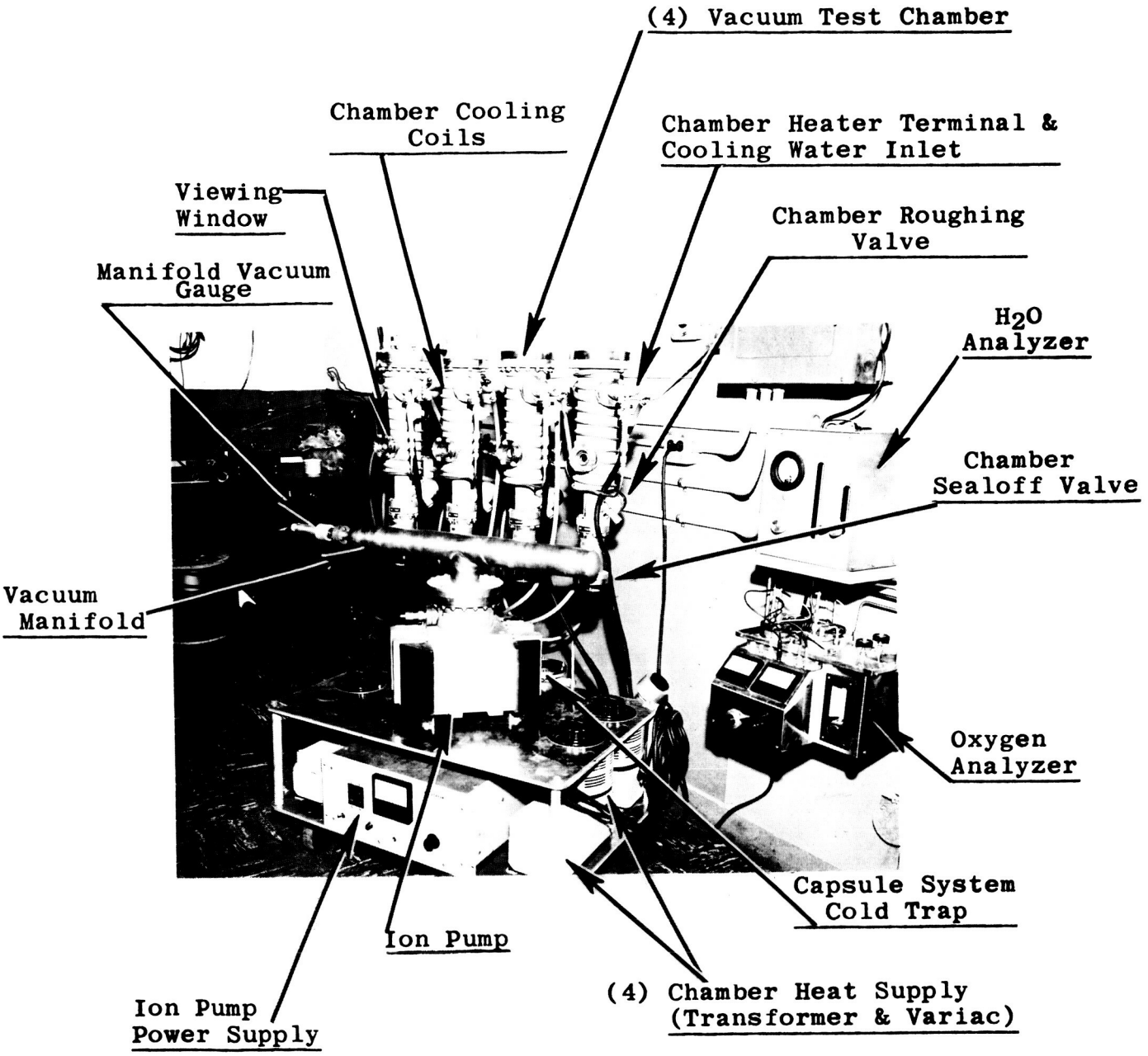

Figure 14

Test Facility

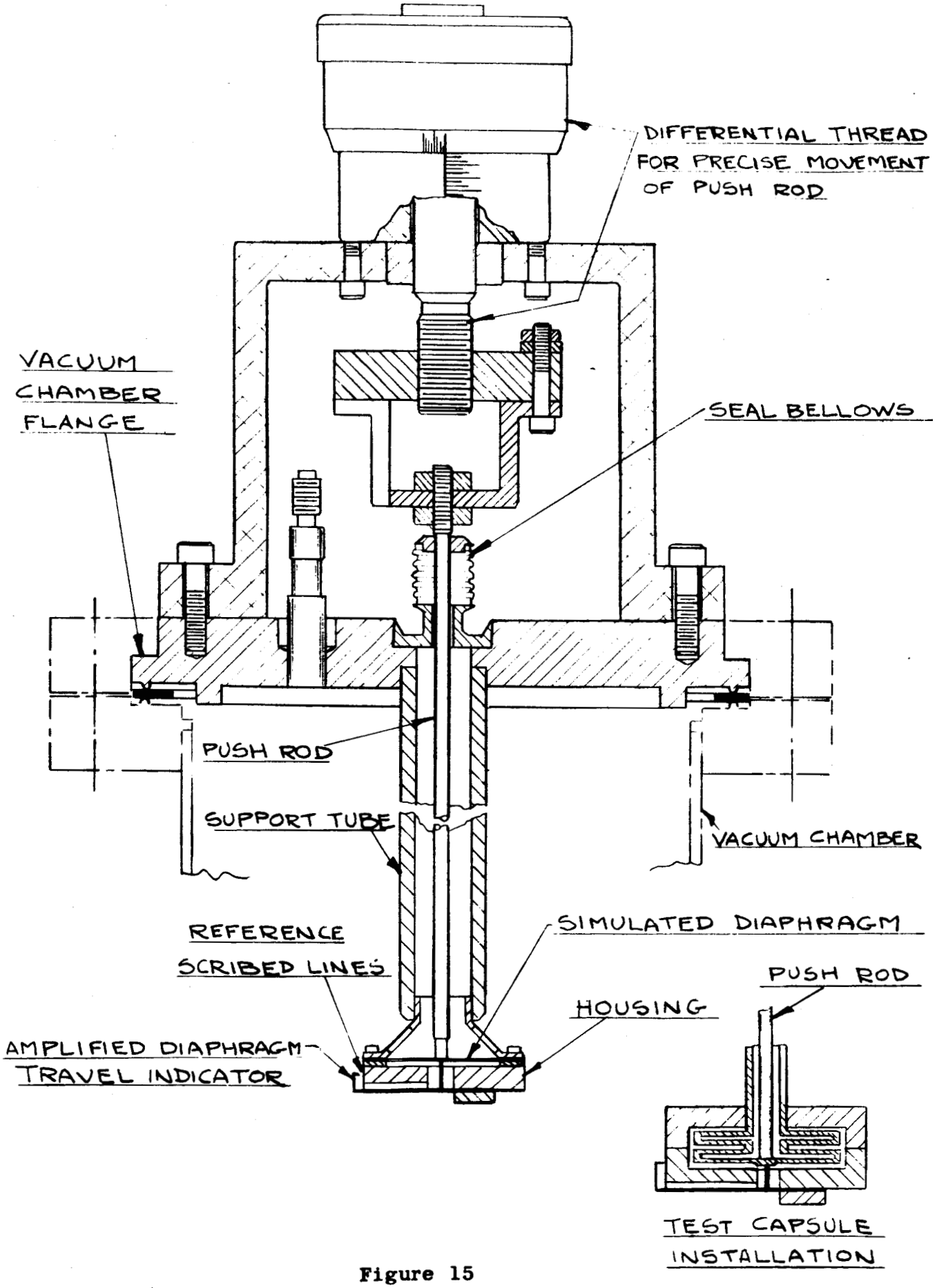

Figure 15

Diaphragm Motion Amplifier System

LIST OF REFERENCES

1. J. J. English, "Binary and Ternary Phase Diagrams of Columbium, Molybdenum, Tantalum, and Tungsten", Defense Metals Information Center Report 152, April 28, 1961 (OTS PB 171421), p. 92

2. Ibid., p. 167

3. R. E. Engdahl, "First Quarterly Report, Pressure Measuring Systems for Closed Cycle Liquid Metal Facilities", NASA CR-54140, July 2, 1964

4. G. L. Kehl, "Principles of Metallographic Laboratory Practice", Third Edition, McGraw-Hill, 1949, p. 92-93

APPENDIX A

NOMENCLATURE

a	Radius of individual turn of pancake coil
A	Thermionic constant, 120 amperes/cm^2 (°K)^2
A_c	Area of capacitor plate
A_e	Thermionic emitter area
B	Thermionic constant
C	Capacitance between pancake coil and diaphragm
C_t	Transmission line capacitance
d	Thermionic emitter-collector distance
d_a	Thermionic emitter - pressure actuated collector distance
d_c	Pancake coil - diaphragm distance
d_r	Thermionic emitter-reference collector distance
e	Electronic charge (1.6 X 10^{-19} coulomb)
E_i	Input voltage to impedance bridge
E_o	Output voltage of impedance bridge
f	Frequency
F.D.	Fineness of detail of objective lens
FL_c	Thermionic collector Fermi level energy

NOMENCLATURE (cont'd)

FL_e	Thermionic emitter Fermi level energy
Gt	Transmission line conductance
H_n	Total axial induction field related to n^{th} turn of pancake coil
H_o	Induction field at center of conductor loop
H_z	Axial induction field component (cylindrical coordinates)
H_ρ	Radial induction field component (cylindrical coordinates
i_a	Thermionic active collector current
i_o	Pancake coil loop current
i_r	Thermionic reference collector current
I	Thermionic current density
$\mathfrak{k}_1', \mathfrak{k}_2'$	Elliptic integrals related to pancake coil
$\mathfrak{k}_1'', \mathfrak{k}_2''$	Elliptic integrals related to image coil
I_c	Current density for critical thermionic emitter
I_s	Saturation emission capability of a surface (current density)
j	$\sqrt{-1}$
K	The Boltzmann Constant (1.38×10^{-23} joule/deg.K)

NOMENCLATURE (cont'd)

L	Pancake coil inductance
L_t	Transmission line inductance
m,n	Indexing parameter
n_r	Index of refraction
N	Number of turns in pancake coil
$N.A.$	Numerical aperture of objective lens
r_i	Inner radius of coaxial cable
r_o	Outer radius of coaxial cable
R_t	Transmission line resistance
s	Distance along transmission line from the input end
S	Transmission line length
S_b	Bartberger factor
t	Time
T	Temperature
T_c	Critical emitter temperature above which space charge occurs
V	Voltage applied to thermionic collector
V_c	Effective emitter-collector potential difference

NOMENCLATURE (cont'd)

V_e	Potential due to thermionic space charge effect
V_m	Voltage generated in individual turn of pancake coil
V_t	Total voltage generated in pancake coil
x_c	Distance from collector to maximum space charge
x_e	Distance from emitter to maximum space charge
X_c	Pancake coil reactance
$2z_e$	Spacing between pancake and image coils
Z_i	Input impedance of transmission line
Z_L	Terminating load impedance of transmission line
Z_o	Characteristic impedance of transmission line
α	Transmission line attenuation constant
β	Transmission line phase constant
γ	Transmission line propagation constant
δ	Skin depth in a medium
δ_e	Skin depth at which field becomes neglible

NOMENCLATURE (cont'd)

ϵ	Dielectric constant of medium =
ϵ_o	Dielectric constant of vacuum (8.854×10^{-12} farad/meter)
ϵ_r	Relative dielectric constant of medium
λ	Wavelength in medium
λ_i	Wavelength of illuminating light
λ_o	Wavelength in vacuum
μ	Permeability of medium =
μ_o	Permeability of vacuum (1.257×10^{-6} henry/meter)
μ_r	Relative permeability of medium
μ_s	Half-angle subtended by objective lens
π	3.1416
ρ_r	Resistivity of material
σ	Conductivity of material
ϕ	Thermionic work factor
ϕ_c	Thermionic collector work function
ϕ_e	Thermionic emitter work function
ϕ_m	Flux linked by individual turn of pancake coil

NOMENCLATURE (cont'd)

ω	Angular frequency = $2\pi f$
(x,y,z)	Cartesian coordinates
(ρ,ϕ,z)	Cylindrical coordinates
(r,θ,ϕ)	Spherical coordinates

APPENDIX B

CALCULATION OF PANCAKE COIL INDUCTANCE

Using the analysis presented in the First Quarterly Report, an effort was made to determine, by slide rule calculations, the inductance of a single turn pancake coil in the presence of a conducting diaphragm. The inductance may be expressed as

$$L = \pi \mu_0 a^2 \int_0^a [F_c - F_i] \rho \, d\rho \qquad \text{(B-1)}$$

where μ_0 is the permeability of vacuum; a is the radius of the current loop; F_c and F_i are functions involving elliptic integrals and dependent upon the parameter a and the cylindrical coordinates z and ρ. The subscripts (c) and (i) refer to pancake coil and image coil parameters respectively. The distance between the pancake and image coils is related to the diaphragm spacing and appears in F_i.

The initial effort involved the use of a spacing of 0.006 inch which decreases to 0.004 inch under pressure. The loop radius was assumed to be a = 0.4 inch. Calculations showed that for this spacing, the difference between the F_c and F_i terms was too small to be evaluated by slide rule and a result was not obtainable.

To remedy the situation, the diaphragm spacing was increased to 0.100 inch and a travel of 0.008 inch under pressure was postulated. Using these parameters, an estimate of L was obtained for a spacing of 0.100 inch. Using a number of values of ρ, it was found that $(F_c - F_i)$ is of a tangent form, changing from zero at $\rho = 0$ to infinity at $\rho = 0.4$. The analytical treatment of the integral involved the adoption of a tangent function in place of $(F_c - F_i)$. It appeared that a reasonable form would be

$$(F_c - F_i) \cong 3 \tan (90\rho/0.4) \text{ degrees} \qquad \text{(B-2)}$$

Using this approach and integrating to $\rho = 0.395$ inch (to avoid the complication of obtaining infinity at $\rho = 0.4$) a value of L = 0.2 microhenry was obtained. If the coefficient of the tangent function is raised to 4 and the integration carried out to $\rho = 0.399$ inch, the value of L becomes 0.5 microhenry. These changes are within reason. Therefore, a range of L would be 0.2 - 0.5 microhenry.

From this point, an effort was made to evaluate the inductance change obtained when the diaphragm

has moved 0.008 inch to a spacing of 0.092 inch. In doing this, it was found that the parameter $(F_c - F_i)$ could be approximated by the same tangent function as before. It must be stressed that this evaluation was obtained by use of a limited number of ρ values and the tangent representation fits equally as well for diaphragm spacings of 0.100 and 0.092 inch. This means that, as far as slide rule calculations can determine, there is no inductance change with diaphragm spacing.

Checking the values of $F_c - F_i)$ for spacings of 0.100 and 0.092 at given values of ρ results in differences starting at about 10 percent for small ρ values and decreasing to about 1 percent as ρ approaches 0.4. Since the value of the integration will depend primarily on large ρ values, the inductance will change by much less than 10 percent. The exact percentage change cannot be determined manually. The integration must be performed on the actual values of $(F_c - F_i)$. This means that

many values of φ must be used and a geometrical determination of the area under the curve must be made. This is most easily and most accurately obtained by computer operations.

In addition to the above statements, it must be remembered that this involved only one current loop. The proposed pancake coil may have as many as 20 turns. Therefore, this calculation must be done 20 times and the results summed up.

It, therefore, appears that the developed impedance analysis can be practically solved only by a computer technique.

APPENDIX C

FINENESS OF DETAIL OF AN OBJECTIVE LENS

According to Kehl (Reference 4), the fineness of detail, or the ability of an objective lens to produce sharply defined separate images of closely spaced detail in the object, is dependent upon the numerical aperture of the objective and the wavelength of light used to illuminate the object. If the aperture of the objective is completely flooded with light, the fineness of detail obtained with the particular objective will be a maximum, and may be expressed as

$$\text{F.D.} = \frac{\lambda_i}{2(\text{N.A.})} \qquad \text{(C-1)}$$

where λ_i is the wavelength of the illuminating light and N.A. is the numerical aperture of the objective.

The numerical aperture may be expressed as

$$\text{N.A.} = \eta_r \sin \mu_s \qquad \text{(C-2)}$$

where η_r is the index of refraction of the medium between the lens and the object and μ_s is one-half the angle subtended by the lens.

If $\mu_s = 30°$, N.A. becomes 0.5 in air ($n_r = 1$). For the binocular microscope at 4 inch working distance, N.A. becomes 0.058. For green light illumination (λ_i = 0.00053 millimeter), the fineness of detail is 0.00053/2(0.058) mm. or 180 microinches.

This result assumes ideal conditions. In the binocular microscope, only one-half of the objective lens is used and the center of the lens is obscured by a mirror. Also the light is not passing through the objective normally, but at a slight angle. Thus a closer approximation would be

$$F.D. = \frac{\lambda_i}{N.A.} \qquad (C-3)$$

resulting in 360 microinches resolution.

Even if a relay microscope at 4 inch working distance were used, the relay telescope would have an N.A. of approximately 0.1 and the microscope would have an N.A. of 0.66. The overall N.A. of the system would be limited to the smallest N.A. of the parts of the system, i.e. N.A. = 0.1.

DISTRIBUTION LIST

Recipient	No. of Copies
National Aeronautics & Space Administration Washington, D. C. 20546 Attention: J. J. Lynch, Code RNP	1
U. S. Atomic Energy Commission Washington, D. C. 20545 Attention: SNAP-50/SPUR Program Office Herbert D. Rochen	1
National Aeronautics & Space Administration Ames Research Center Moffett Field, California 94035 Attention: Library	1
National Aeronautics & Space Administration Goddard Space Flight Center Greenbelt, Maryland 20771 Attention: Library	1
National Aeronautics & Space Administration Jet Propulsion Laboratory 4800 Oak Grove Drive Pasadena, California 91103 Attention: Library	1
National Aeronautics & Space Administration Langley Research Center Langley Station Hampton, Virginia 23365 Attention: Library	1

DISTRIBUTION LIST (CONTINUED)

Recipient	No. of Copies
National Aeronautics & Space Administration Lewis Research Center 21000 Brookpark Road Cleveland, Ohio 44135	
Attention: Library (3-7)	2
Technology Utilization Office(15-1)	1
Office of Reliability & Quality Assurance (21-4)	1
Dr. B. Lubarsky (500-201)	1
R. F. Mather (500-309)	1
R. N. Weltmann (500-309)	2
R. R. Miller (500-201)	1
H. P. Odom (500-201)	1
M. J. Saari (500-202)	1
C. C. Gettelman (77-1)	1
D. R. Englund, Jr. (77-1)	1
Dr. L. Rosenblum (106-1)	1
H. H. Christenson (5-3)	1
J. E. Dilley (500-309)	1
M. O. Dustin (54-1)	1
E. A. Koutnik (500-201)	1
National Aeronautics & Space Administration George C. Marshall Space Flight Center Huntsville, Alabama 35812	
Attention: Library	1
National Aeronautics & Space Administration Scientific & Technical Information Facility P. O. Box 5700 Bethesda, Maryland 20014	
Attention: NASA Representative	6

DISTRIBUTION LIST (CONTINUED)

Recipient	No. of Copies
Air Force Systems Command Aeronautical Systems Division Wright-Patterson AFB, Ohio 45433	
Attention: Library (EWABE)	1
C. H. Armbruster (APlP)	1
U. S. Atomic Energy Commission CANEL Project Office P. O. Box 1102 Middletown, Connecticut 06458	
Attention: W. H. Pennington	1
Argonne National Laboratory P. O. Box 299 Lemont, Illinois 60439	
Attention: Library	1
Brookhaven National Laboratory Upton, New York 11973	
Attention: Library	1
Dr. O. E. Dwyer	1
Oak Ridge National Laboratory Oak Ridge, Tennessee 37831	
Attention: Dr. H. W. Hoffman	
Y-12 Site, Building 9204-1	1
Aerojet-General Corporation SNAP-8 Division Azusa, California 91703	
Attention: Dr. C. C. Ross	1
The Bendix Corporation Research Laboratories Division Southfield, Michigan	
Attention: G. A. Rosselot	1

DISTRIBUTION LIST (CONTINUED)

Recipient	No. of Copies
Data Sensors, Incorporated 13112 Crenshaw Boulevard Gardena, California Attention: J. M. DeStefano	1
Electro-Optical Systems, Inc. 300 N. Halstead Street Pasadena, California Attention: Dr. J. M. Teem	1
Endevco Corporation 801 South Arroyo Parkway Pasadena, California Attention: Library	1
General Electric Company Missile and Space Division Space Power & Propulsion Section Cincinnati, Ohio 45215 Attention: E. Schnetzer	1
General Motors Corporation Allison Division P. O. Box 894 Indianapolis, Indiana 46206 Attention: Dr. F. G. Meyers	1
Gulton Industries, Incorporated Instrumentation Division 212 Durham Avenue Metuchen, New Jersey Attention: Dr. W. Welkowitz	1
Kulite-Bytrex Corporation 50 Hunt Street Newton, Massachusetts 02158 Attention: Dr. A. D. Kurtz	1

DISTRIBUTION LIST (CONTINUED)

Recipient	No. of Copies
West Coast Research Corporation 2102 South Sepulveda Boulevard Los Angeles, California 90025 Attention: H. M. Spivack	1
Westinghouse Electric Corporation Astronuclear Laboratory P. O. Box 10864 Pittsburgh, Pennsylvania 15236 Attention: W. D. Pouchot	1
North American Aviation, Incorporated Atomics International Division P. O. Box 309 Canoga Park, California 91303 Attention: Dr. L. Bernath	1
AiResearch Manufacturing Company Division of the Garrett Corporation 402 South 36th Street Phoenix, Arizona 85034 Attention: J. Dennan	1
Ford Instrument Company Division of the Sperry Rand Corporation 31-10 Thomson Avenue Long Island City 1, New York Attention: Don Gertz	1

DISTRIBUTION LIST (CONTINUED)

Recipient	No. of Copies
Materials Research Corporation Orangeburg, New York 10962 Attention: Dr. G. T. Murray	1
McGraw-Edison Company Thomas A. Edison Research Laboratory West Orange, New Jersey Attention: M. D. Bowers	1
MSA Research Corporation Callery, Pennsylvania 16024 Attention: Dr. R. C. Werner	1
North American Aviation, Incorporated Rocketdyne Division 6633 Canoga Avenue Canoga Park, California 91303 Attention: J. L. Armstrong	1
Physical Sciences Corporation 314 East Live Oak Avenue Arcadia, California Attention: J. L. Roshala	1
Trans-Sonics, Incorporated Pressure Instrumentation Division Burlington, Massachusetts Attention: R. E. Jackson	1
United Aircraft Corporation Pratt & Whitney Aircraft Division CANEL, P. O. Box 611 Middletown, Connecticut 06458 Attention: Library	1